Quantitative Assessment of Anterior Segment Inflammation in a Rat Model of Uveitis Using Spectral-Domain Optical Coherence Tomography

Kathryn L. Pepple,[1] Woo June Choi,[2] Leslie Wilson,[1] Russell N. Van Gelder,[1,3,4] and Ruikang K. Wang[2]

[1]Department of Ophthalmology, University of Washington, Seattle, Washington, United States
[2]Department of Bioengineering, University of Washington, Seattle, Washington, United States
[3]Department of Biological Structure, University of Washington, Seattle, Washington, United States
[4]Department of Pathology, University of Washington, Seattle, Washington, United States

Correspondence: Kathryn L. Pepple, Department of Ophthalmology, Campus Box 359608, University of Washington, 325 9th Avenue, Seattle WA 98104, USA; kathryn.pepple@gmail.com.

Submitted: February 2, 2016
Accepted: May 29, 2016

Citation: Pepple KL, Choi WJ, Wilson L, Van Gelder RN, Wang RK. Quantitative assessment of anterior segment inflammation in a rat model of uveitis using spectral-domain optical coherence tomography. *Invest Ophthalmol Vis Sci*. 2016;57:3567–3575. DOI:10.1167/iovs.16-19276

Purpose. To develop anterior segment spectral-domain optical coherence tomography (SD-OCT) and quantitative image analysis for use in experimental uveitis in rats.

Methods. Acute anterior uveitis was generated in Lewis rats. A spectral domain anterior segment OCT system was used to image the anterior chamber (AC) and ciliary body at baseline and during peak inflammation 2 days later. Customized MatLab image analysis algorithms were developed to segment the AC, count AC cells, calculate central corneal thickness (CCT), segment the ciliary body and zonules, and quantify the level of ciliary body inflammation with the ciliary body index (CBI). Images obtained at baseline and during peak inflammation were compared. Finally, longitudinal imaging and image analysis was performed over the 2-week course of inflammation.

Results. Spectral-domain optical coherence tomography identifies structural features of inflammation. Anterior chamber cell counts at peak inflammation obtained by automated image analysis and human grading were highly correlated ($r = 0.961$), and correlated well with the histologic score of inflammation ($r = 0.895$). Inflamed eyes showed a significant increase in average CCT (27 μm, $P = 0.02$) and an increase in average CBI ($P < 0.0001$). Longitudinal imaging and quantitative image analysis identified a significant change in AC cell and CBI on day 2 with spontaneous resolution of inflammation by day 14.

Conclusions. Spectral-domain optical coherence tomography provides high-resolution images of the structural changes associated with anterior uveitis in rats. Anterior chamber cell count and CBI determined by semi-automated image analysis strongly correlates with inflammation, and can be used to quantify inflammation longitudinally in single animals.

Keywords: uveitis, animal model, optical coherence tomography, inflammation, anterior chamber

Uveitis, or ocular inflammation, can lead to significant visual impairment in up to 30% of affected individuals, and is responsible for approximately 10% of blindness in the United States and other western countries.[1,2] Anterior uveitis is the most common form of uveitis in humans, and is characterized by changes in the anterior chamber (AC) including infiltration of inflammatory cells and an increase in the protein concentration of the aqueous humor (flare). Ocular exam by slit lamp ophthalmoscopy is the current standard methodology for monitoring the AC in patients with uveitis. The degree of cell and flare is scored according to a consensus grading system known as the Standardization of Uveitis Nomenclature (SUN) criteria.[3] Changes in SUN criteria cell and flare over time are indicative of disease progression or response to therapy.

In rodent models of uveitis, the small size of the eye makes clinical scoring of AC inflammation in vivo challenging, leading to the use of histology to assess endpoints. Using histology to study disease progression over time requires the use of cohorts of animals killed at prespecified time points, and is not compatible with longitudinal evaluation in a single animal. In addition, tissue processing for histology can introduce artifacts that can complicate structural evaluation in the postmortem eye.[4] Optical coherence tomography (OCT) is a noninvasive in vivo imaging modality that provides structural information with micrometer-resolution, and can be performed repeatedly on a single animal. Retinal OCT has been described for use in the mouse model of experimental autoimmune uveitis (EAU),[5–8] and analysis of AC OCT in humans has been compared to clinical scoring in patients with anterior uveitis.[9–11] However, to date anterior segment OCT has not been widely utilized in rodent models of uveitis. The goal of the present study was to determine if anterior segment OCT imaging in rodents could accurately detect inflammation when compared to histology. The long-term goal of this work is to use automated analysis of anterior segment OCT images to develop a quantitative score that can detect the changes in inflammation over time in a single animal.

Methods

Animals and Uveitis Induction

The animal study protocol was approved by the Animal Care and Use Committee of the University of Washington (animal study protocol # 4184-04) and was compliant with the ARVO Statement for the Use of Animals in Ophthalmic and Vision Research.

Female Lewis rats ($N = 11$) weighing 180 to 200 g were purchased from Harlan Laboratories and maintained with standard chow and water ad libitum under specific pathogen-free conditions. Acute uveitis was initiated in the right eye of each animal with intravitreal injection of 10 μg of killed mycobacterium tuberculosis H37Ra antigen (Difco Laboratories, Detroit, MI, USA) in a 5-μL volume of phosphate-buffered saline (PBS) on day 0. Corticosteroid-treated animals also received a periocular injection of 4 mg triamcinolone in 100 μL on day 0. Imaging was performed on day 0 prior to injection, and at the peak of inflammation on day 2 for rats 1 to 9. For rats 10 and 11, imaging was also performed on days 4, 7, and 14. During injections and OCT imaging, animals were anesthetized with inhaled 2% to 5% isoflurane.

Histology

For histology, right eyes were harvested after OCT imaging at day 2 or day 14, placed in 4% paraformaldehyde for 48 hours, and then embedded in paraffin blocks. Four-millimeter sections were stained with hematoxylin and eosin (H&E). On each section, the number of cells was determined for three nonoverlapping anatomic locations: the AC, the posterior chamber and area surrounding the ciliary body, and in the vitreous. Cells were counted on three sections per animal for rats 1, 4, 6, 7, 8, and 9.

Spectral-Domain OCT System and Image Acquisition

The anterior segment OCT system used in this study was previously described by our group.[12,13] In brief, it is a custom-built SD-OCT operated at a wavelength of 1340 nm and a scan speed of 92,000 A-scans per second. The spatial (axial × lateral) resolution of system was 7×7 μm in air. The system sensitivity was ~ 105 dB at the focus spot of the sample beam corresponding to 0.5 mm below the zero delay line. Each animal was placed in the right lateral decubitus position and secured in a custom-made stereotactic stage equipped with a heating pad and a nose cone for continuous inhaled isoflurane anesthesia. Corneal protection was provided with a topical balanced salt solution (BSS; Alcon, Johns Creek, GA, USA) throughout the imaging session.

Image Analysis of the Cornea, AC, and Ciliary Body

AC Segmentation. A three-dimensional (3D) scan consisting of equally spaced 400 B-scans (512 A-lines/B-scan) was obtained for each eye, covering a field of view of 2.6×2.6 mm or 4.5×4.5 mm depending on the ocular regions to be analyzed. Semi-automated image analysis was performed on 20 B-scan images within the 3D scan at regularly spaced intervals across the AC (approximately every 20th B-scan). If significant reflection artifact was present in the selected B-scan image, then the nearest adjacent image without artifact was used. The boundaries of the AC were identified using a semi-automated segmentation method adapted from a retinal segmentation method previously published.[14] In brief, the region of the AC was defined by manually placing two lines along the posterior corneal boundary and upper boundaries of iris and lens on one image. A double line model (DLM) based edge detector algorithm[14] was then automatically guided by these sketched lines to track and segment the user-defined region in additional images.

AC Cell Counting. Manual cell counting was performed by an expert grader (KP) using Adobe Photoshop (San Jose, CA, USA) to visualize and mark cells.

Automated cell counting was performed after AC segmentation using a customized MatLab algorithm. Cell candidates within the AC were defined as at least two adjacent pixels with an intensity greater than a prespecified threshold. The threshold was defined as the average of background pixel intensity (BG_Mean) plus two times the standard deviation of BG_Mean (BG_STD). Therefore, a cell was defined as adjacent pixels with an intensity > BG_Mean+2*BG_STD. The background was defined using a 20×20 pixel area, where only air is present in the OCT image (close to zero delay line).

Corneal Segmentation. Central corneal thickness (CCT) was determined for the 2.58×2.58 mm region centered on the pupil (300×236 pixels). The pupil was identified in the en face volume intensity projection of the 3D OCT image set for each rat eye. To identify the corneal boundaries, the user-guided retinal segmentation algorithm was modified to identify the epithelial/air and endothelial/AC boundaries. Once segmented, the profile of corneal thicknesses across the central cornea was determined by calculating the normal distance between top and bottom corneal boundaries.

Ciliary Body Index (CBI) Determination. The central scan through the pupil was identified and analyzed along with 10 scans, flanking the scan on either side (total = 21 central scans analyzed). Ciliary body index was determined for each animal on day 0 and day 2. To determine the CBI, the ciliary body and zonules were isolated in a user-defined ellipse mask placed in the region posterior to the iris, adjacent to the lens capsule, and adjacent to the inner scleral wall. Pixel intensity within the ellipse was transformed into a binary value of 1 if the intensity was above two times an average of background intensity (BG_Mean). The ciliary body index was then determined as the ratio of the number of pixels with a value of 1 to the total number of pixels in the ellipse (CBI = # pixels of value 1/total # of ellipse pixels).

Statistical Analysis

The difference between inflamed and corticosteroid treated cell counts by histology, and the differences in longitudinal average AC cell count and CBI were determined using Kruskal-Wallis 1-way analysis of variance (ANOVA) and post hoc pairwise comparisons with a Bonferroni correction for multiple comparisons. The difference between human and automated cell counting and ciliary body densities on day 0 and day 2 were determined using a Wilcoxon matched pairs signed rank test. The correlation between human and automated analysis for counting AC cell, and between AC cell count by histology and automated analysis of AC OCT images were determined using a Spearman's rank correlation coefficient. Analyses were performed with Prism 6 graph pad software. Significance was determined for $P < 0.05$.

Results

SD-OCT Detects Inflammatory Structural Changes in the AC and Around the Ciliary Body

To determine if anterior segment SD-OCT could detect the presence of inflammation in the rat eye, images were obtained

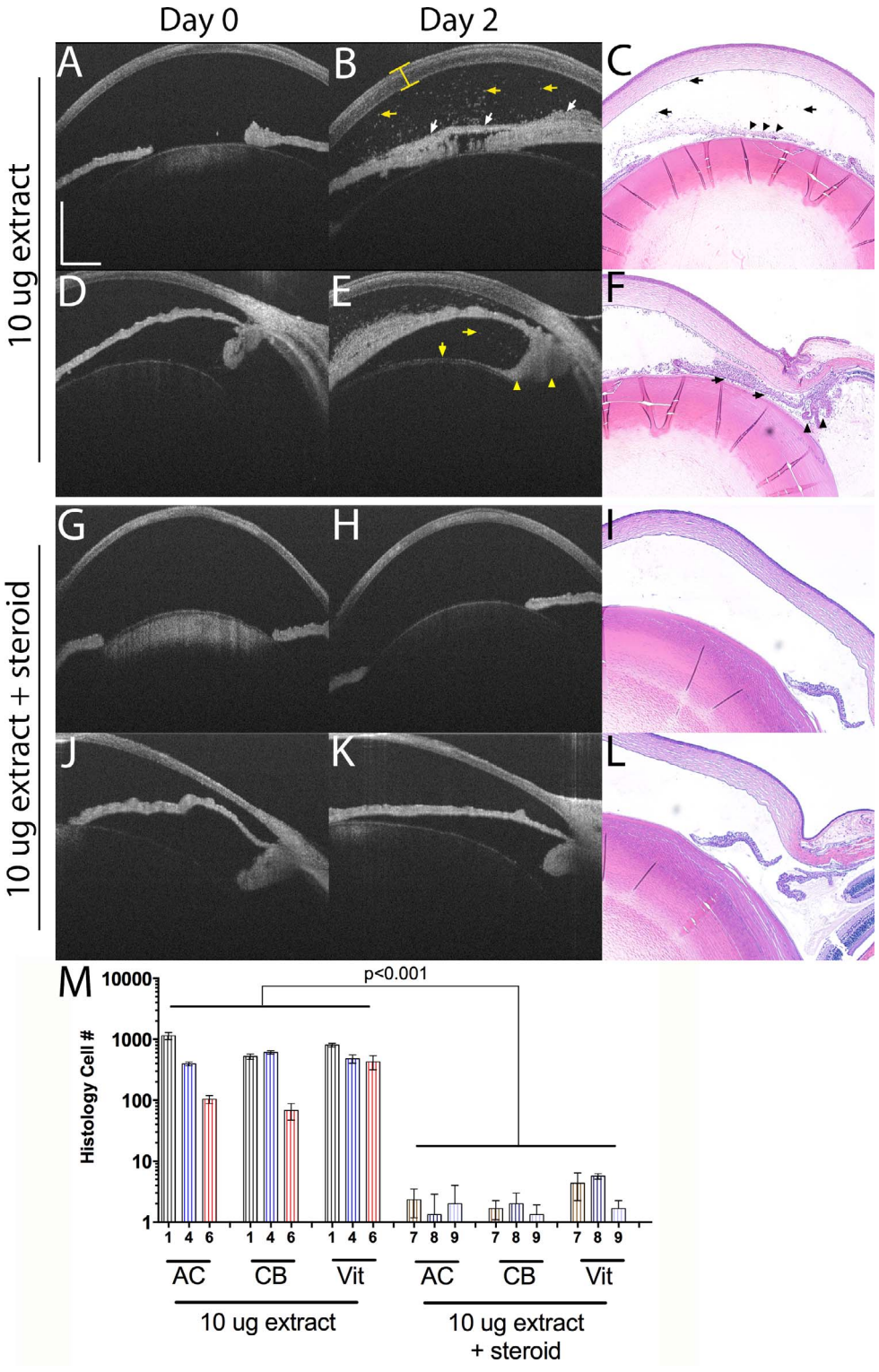

Figure 1. In vivo anterior segment OCT demonstrates inflammatory structural changes in the rat eye. (**A**) Day 0 central AC centered image of rat 1. *Scale bar*: 500 μm in both directions with adjustment for index of refraction. (**B**) Day 2 central AC centered image of rat 1 demonstrates corneal edema (*yellow bars*), AC cell (*yellow arrows*), and a pupillary membrane (*white arrows*). (**C**) Day 2 histology confirms the presence of AC cell (*black arrows*) and pupillary membrane (*three black arrowheads*). (**D**) Day 0 limbus centered image of rat 1 visualizes the ciliary body, the anterior lens capsule, and the posterior chamber (area between the lens and the iris. (**E**) Day 2 limbus centered image of rat 1 identifies cells in the posterior chamber and along the anterior lens capsule (*yellow arrows*). There is also increased reflectivity of the ciliary body and zonules compared with day 0 (*yellow arrowheads*). (**F**) Day 2 histology confirms the presence of cells in the posterior chamber (*black arrows*), and infiltration of inflammatory cells surrounding the ciliary body (*black arrowheads*). Day 0 AC centered (**G**) and limbus centered (**J**) images of rat 7. Day 2 AC centered (**H**) and limbus centered (**K**) images of rat 7 demonstrate the absence of inflammation in the presence of corticosteroid treatment. Day 2 histology of rat 7 AC (**I**) and limbus (**L**) confirms the absence of inflammation. (**M**) Graph of cells counted in the AC, the posterior chamber and ciliary body (CB), and in the vitreous (Vit) from histologic sections for rats 1, 4, 6, 7, 8, and 9.

Investigative Ophthalmology & Visual Science

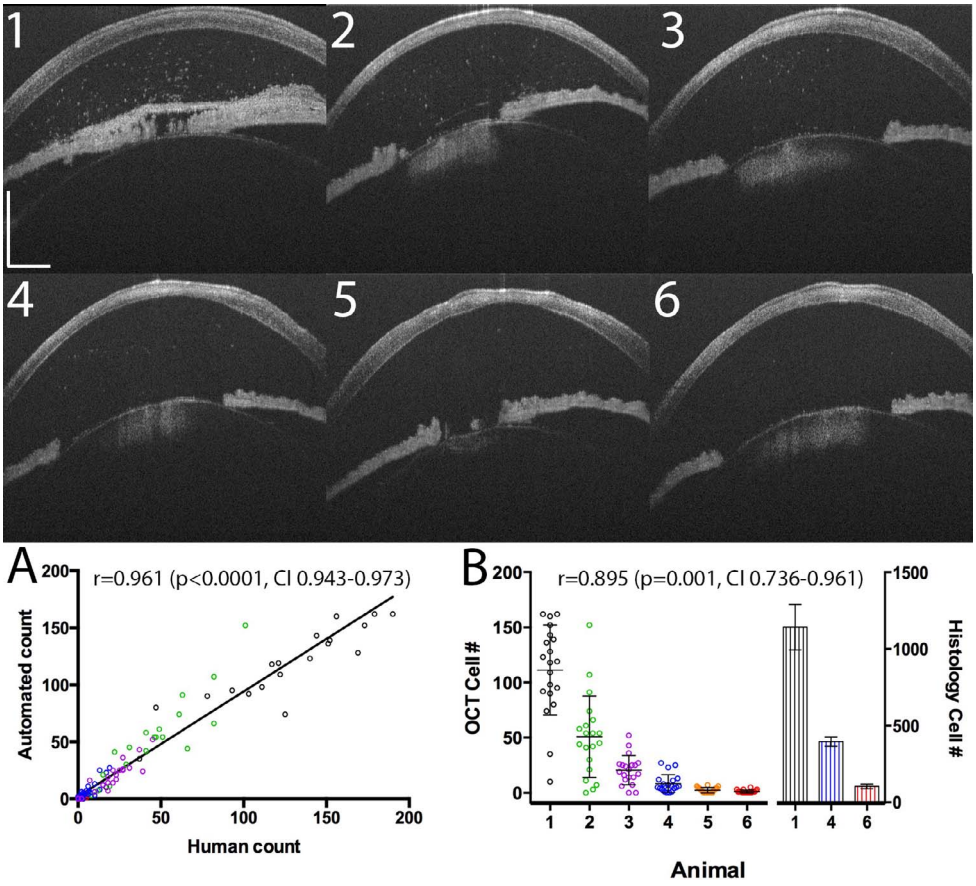

Figure 2. Quantification of AC cell by semiautomatic image analysis agrees with a human grader and identifies a wide range of inflammation. (**1–6**) Representative images of central OCT B-scans from the six inflamed rats (treated with 10 μg extract) on day 2. *Scale bar*: 500 μm in both directions with adjustment for index of refraction. (**A**) Graph comparing AC cell counts obtained from AC centered OCT images by semi-automated analysis and a human grader. (**B**) Left graph shows the number of cells counted from each of 20 B-scan images for each animal (1–6) on day 2. Right graph shows the number of cells counted in the AC from histologic sections for animals 1, 4, and 6. Bars indicate the mean and standard deviation.

on day 0 (baseline) and day 2 (inflamed) and compared (Fig. 1). Two sets of images were obtained for each animal on each day. The first set was centered on the AC; the second set was centered on the limbus. Comparison of images from day 0 (Figs. 1A, 1D) and day 2 reveals structural changes of inflammation including corneal edema, AC cell, pupillary membrane, and ciliary body inflammation (Figs. 1B, 1E). These signs of inflammation were confirmed by histology (Figs. 1C, 1F). The signs of inflammation were not observed in SD-OCT images or by histology in corticosteroid treated animals (Figs. 1G–L). Inflammation was quantified by histology for three mycobacteria-treated animals, and three mycobacteria + corticosteroid-treated animals (Fig. 1M). Inflammatory cells were counted in the AC, surrounding the ciliary body, and in the vitreous for three sections per animal. The difference between cell counts in inflamed and corticosteroid treated eyes was significantly different ($P < 0.001$). Among the inflamed eyes, there was a wide range of cells counted, particularly in the AC and CB. Rat 1 demonstrated the most inflammation with an average number of cell/section = 822. Rat 6 demonstrated the least inflammation with an average of 199 cells/section. Rat 4 fell in between these two with an average of 495 cells/section. The corticosteroid treated eyes from rats 7, 8, and 9 had substantially fewer cells with an average of eight, nine, and five cells/section respectively.

Image Analysis for Quantitative AC Cell Counting Correlates Strongly With Human Cell Counting and Well With Histologic Cell Counts

Anterior chamber centered SD-OCT images were obtained on six inflamed rats (Fig. 2 images 1–6). In order to quantify the number of AC cells present, a MatLab program was developed to segment the AC and count hyperreflective cells within the segmented boundary. On 20 images spaced evenly across the AC for these six animals (generating a total of 120 scored images), cells were also counted by a human grader and compared to the cell numbers obtained by the MatLab algorithm. There was no significant difference between the cell counts obtained by the algorithm and human grader ($P = 0.299$). Over a wide range of cells, there was excellent correlation between human and automated scoring with a Spearman's rho = 0.961($P < 0.0001$; confidence interval [CI]: 0.9437–0.9729; Fig. 2A). A wide range of AC cell was detected as seen in the scatter plots graphs of the cell counts generated from the 20 SD-OCT images per rat (Fig. 2B).

To determine how well cell counts obtained from SD-OCT images correlate with cell counts obtained by histology, AC cells were counted on three central pupillary-optic nerve (P-O) histology sections for animals 1, 4, and 6 and were compared with the number of cells counted in three central SD-OCT scans (Table). Overall, the number of cells counted by

Investigative Ophthalmology & Visual Science

Table. Comparison of the Number of AC Cells by Histology and OCT

	1			4			6		
Histology	989	1285	1153	361	417	408	92	98	121
OCT	190	152	151	15	19	17	3	5	5

$r = 0.895$
CI: 0.736–0.961

histology was much higher than counted by OCT. Despite the difference in scale, there was strong correlation between the number of cells counted on histologic sections with automated counts in central B-scans, Spearman's rho 0.895 ($P = 0.001$; CI: 0.736–0.961; Fig. 2B).

Image Analysis for Quantitative Measurement of Corneal Thickness Identifies Edema in Association With Inflammation

Anterior chamber inflammation is associated with corneal edema in humans and animal models of uveitis.[10,15] In order to determine if changes in rat corneal thickness could be identified and quantified on OCT, CCT was determined on day 0 and day 2 for each injected eye. After scanning, en face thickness maps of the CCT (centered on the pupil) were generated, which highlight regional variations in thickness (Figs. 3A–D). Average CCT across the volume scan for day 0 and day 2 were then calculated and compared (Fig. 3E). On average, CCT increased by 27 μm (21%) with inflammation and this difference was significantly different from baseline ($P = 0.02$). In the presence of corticosteroid treatment, CCT decreased by 11 μm (11%) on day 2, but this difference was not significant ($P = 0.71$).

CBI As a Measurement of Ciliary Body and Zonule Inflammation

Ciliary body inflammation can be detected in experimental animals by histology, but no method for in vivo detection of ciliary body inflammation has been previously described. As the Lewis rat strain is albino, the ciliary body can be visualized in OCT images centered at the limbus (Fig. 4). In order to visualize inflammatory changes, day 0 and day 2 limbus-centered images were compared for the six inflamed animals and the three corticosteroid treated animals. Inflamed eyes were noted to have cells on the anterior lens capsule, cells in the posterior chamber (area between the anterior lens capsule and the iris), increased hyperreflectivity in the area of the zonules, and an enlarged ciliary body. In order to quantify these changes, a region of interest (ROI) containing the ciliary body and zonules was identified (white ellipses in Fig. 4) and the CBI was determined as the ratio of hyperreflective pixels to total pixels in the ROI. The ciliary body index for 21 central images per animal on day 0 and day 2 were calculated and compared. The average baseline CBI for all nine animals was 0.2511 ± 0.0457. When separated by treatment (Fig. 4A), the average baseline CBI for the six inflamed animals was 0.2566, which increased significantly to an average CBI of 0.3440 on day 2 ($P < 0.0001$). The ciliary body index for corticosteroid-treated animals was not significantly different on day 2 (average CBI 0.2390) when compared to day 0 (average CBI 0.2402; $P = 0.7$). Next we looked at the CBI changes for each individual animal (Fig. 4B). The ciliary body indexes on day 2 increased for all inflamed rats, with a significant increase in inflammation noted for rats1, 2, 4, 5, and 9 ($P < 0.0001$). The difference for rats 3 and 6 were not significant after correction for multiple comparisons. No clear pattern emerged for corticosteroid treated animals. Rat 7 had no change in CBI, rat 8 had a significant decrease in average CBI, and rat 9 had a significant increase in average CBI.

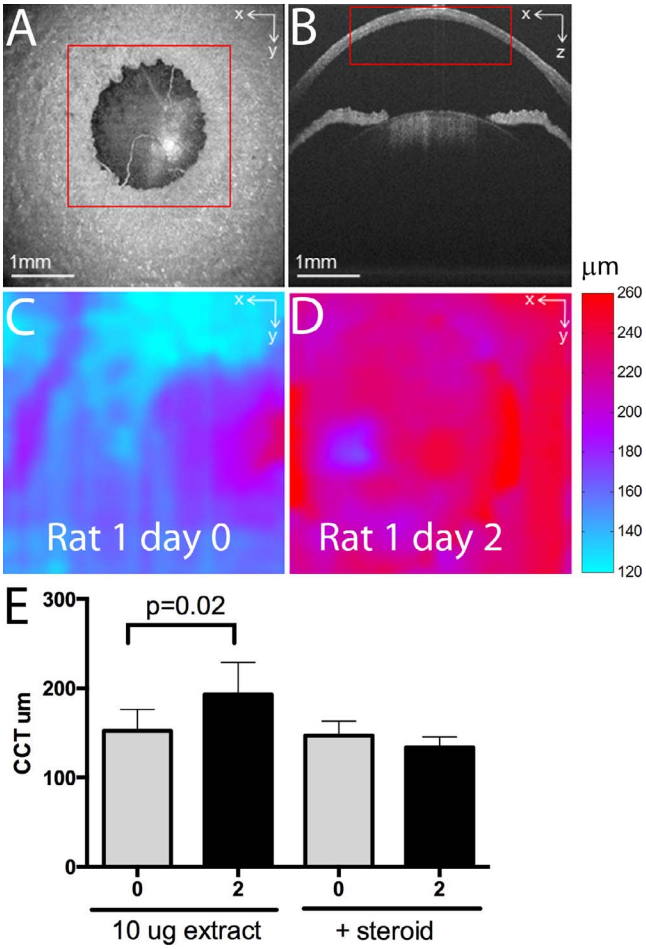

Figure 3. Quantification of average CCT from AC centered OCT images identifies increased thickness with inflammation. (**A**) The center of the pupil is identified in the OCT generated volume intensity projection image and used to define the center of the cornea. (**B**) The central cornea thickness is determined for the 2.58 × 2.58 mm^2 region centered on the pupil (*red box*). Corneal images within this region are segmented to define the epithelial and endothelial boundaries, and the distance between the boundaries determined. (**C**) An en face thickness map of the CCT for rat 1 on day 0. (**D**) En face thickness map of rat 1 on day 2. (**E**) Average corneal thickness on day 0 (*gray bar*) and day 2 (*black bar*) comparing CCT for all inflamed and corticosteroid treated animals.

Longitudinal Quantification of AC Cell and CBI in the Same Animal Detects Significant Changes With Peak Inflammation

To determine if quantification of OCT imaging could identify a change in inflammation in a single animal over the course of inflammation, uveitis was induced in two animals (rats 10 and 11), and imaging performed on days 0, 2, 4, and 14 (Fig. 5). Both animals demonstrated peak inflammation on day 2 that resolved by day 14, which is consistent with our previously published data on this uveitis model.[16,17] For both animals, the increase in AC cell (Figs. 5A, 5C) and CBI (Figs. 5B, 5D) on day 2 was significantly increased over baseline, and returned to baseline levels by day 14. Rat 10 demon-

Investigative Ophthalmology & Visual Science

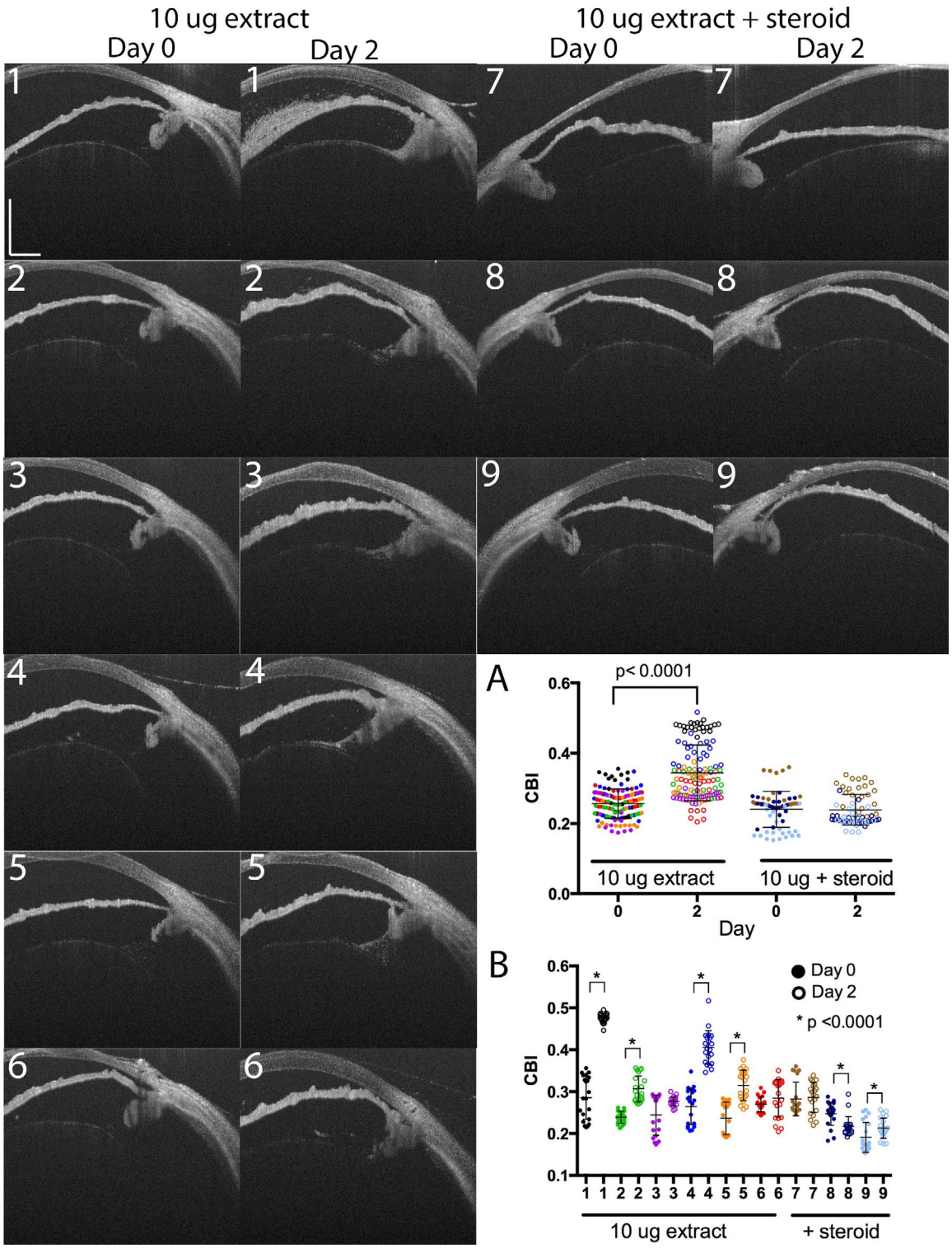

Figure 4. Quantification of ciliary body inflammation using the CBI. (**1–9**) Representative images of limbus-centered OCT images from the six inflamed (**1–6**) and three corticosteroid treated (**7–9**) rats on day 0 (*left panels*) and day 2 (*right panels*). *Scale bar*: 500 μm in both directions with adjustment for index of refraction. The *elipse* outlines the user-defined region of interest containing the ciliary body and zonules from which the CBI was determined. (**A**) Graph showing the significant increase in the CBI from day 0 and day 2 for rats 1 to 6. The difference between the day 0 and day 2 CBI for corticosteroid treated animals (**7–9**) was not significant ($P = 0.71$). (**B**) Comparison of the CBI on day 0 and day 2 for individual animals. * $P < 0.0001$. *Filled circles* indicate day 0, and *empty circles* indicate day 2.

strated more qualitative inflammation than rat 11 on day 2 as evidenced on OCT by more visible AC cell and the presence of a pupillary membrane. This difference was also captured quantitatively with a significantly higher AC cell counts for rat 10 (average 81 cells/image) compared with rat 11 (average 2 cells/image; $P < 0.001$). Average CBI on day 2 was also significantly higher in rat 10 (0.35) compared with rat 11 (0.30) $P < 0.0001$.

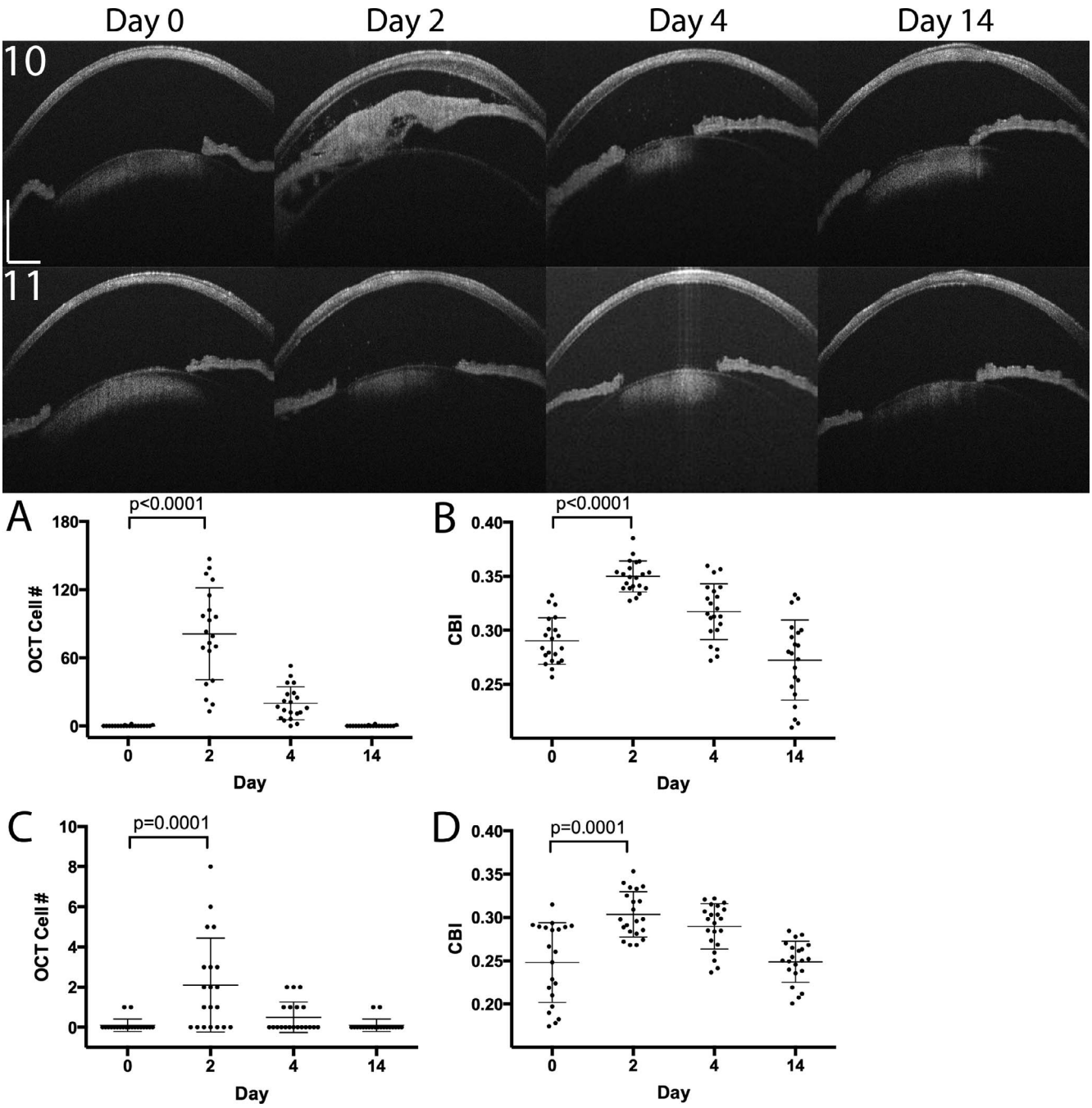

Figure 5. Longitudinal OCT image analysis provides quantification of inflammation over time in individual animals. (**10**, **11**) Representative images of AC centered images from two inflamed rats (**10**, *top row*) and (**11**, *bottom row*) obtained on days 0, 2, 4, and 14. *Scale bar*: 500 µm in both directions with adjustment for index of refraction. (**A**) AC cell count and (**B**) CBI on each day for rat 10. (**C**) AC cell count and (**D**) CBI on each day for rat 11.

Discussion

Optical coherence tomography imaging provides in vivo micron level resolution analysis of ocular structures in health and disease.[18] We show here in a rat model of anterior uveitis that AC cell count and CBI generated by semi-automated analysis of anterior segment OCT correlates strongly with histologic inflammation and human grading, and can be used to quantitate inflammation longitudinally in single animals.

Anterior chamber cell is a key marker of inflammation in humans, but has been difficult to evaluate in vivo in animal models. To our knowledge, only one previous report of in vivo AC cell counting by SD-OCT has been published.[19] In this report analyzing a mouse keratitis model, AC cell counting was performed manually. One goal of the work presented in this report is to develop a process for automated image analysis that would obviate the need for the labor- and time-intensive process required for manual grading. We show here that the cell counting algorithm was robust, generating cell counts that strongly correlated with human counts over a wide range of inflammation. Determining the precision and accuracy of a new surrogate for ocular inflammation is important. We found the precision of our OCT algorithm was good with less than a

Investigative Ophthalmology & Visual Science

2% difference between the total number of cells counted on all images by the human grader (3963 cells) and the algorithm (3886 cells). However, absolute cell counts obtained from histology and OCT were quite different. Therefore, at this time, we can only consider OCT cell counts as a conservative estimate of the true number of AC cells in vivo. Accuracy of OCT cell counting is significantly affected by the distribution of cells in the AC. Only free-floating cells within the central AC were counted by our automated method. Image analysis did not identify individual cells when they were adherent to the corneal endothelium or anterior surface of the iris. Instead, these cells were included in the segmentation boundary of the AC. In addition, cells present in the extremes of the iridocorneal angles were not imaged by OCT. Determination of accuracy may also have been impacted by the use of histology as the gold standard. It is not known to what degree histology introduces artifacts such as postmortem extravasation of white blood cells to the AC or disruption of inflammatory membranes with cell liberation. Ultimately, a better gold standard is needed to determine accuracy, such as a large animal or human model that could be evaluated in vivo by OCT and by SUN criteria or AC paracentesis and cell counting. Despite these limitations, OCT was able to accurately detect the difference between high and low levels of absolute inflammation as determined by histology.

Ciliary body inflammation has been identified by histology in experimental models of uveitis, such as endotoxin-induced uveitis (EIU),[20] experimental autoimmune anterior uveitis (EAAU),[21] and primed mycobacterial uveitis (PMU).[16] It has been proposed that the ciliary body may function as a central conduit for the efflux of inflammatory cells across the blood aqueous barrier and into the intraocular space. However, no in vivo measurement of ciliary body inflammation has been previously described to further explore this hypothesis. Spectral-domain optical coherence tomography imaging offers the potential to look for changes in the ciliary body and posterior chamber that may precede AC chamber inflammation. In this study, we were interested to find that there was not always a direct association between the degree of inflammation detected by changes in the CBI and AC cell. For example, rats 4 and 5 had significant increases in CBI, but less impressive changes in AC cell count. This could support the ciliary body egress hypothesis. Alternatively, this could be a unique finding in PMU due to the intravitreal injection of the inflammatory stimulus. Further studies in multiple models of anterior uveitis using SD-OCT to assess and monitor the ciliary body changes over time will help clarify the importance of this finding.

Corneal edema in the setting of AC inflammation has been identified using SD-OCT in humans[10] and in experimental models of keratitis in mice.[19] This is consistent with our finding that CCT increased on average in the inflamed animals, but not in animals treated with corticosteroid. Prior studies of corneal thickness in Lewis rats using histology identified a postprocessing corneal thickness of 126.89 ± 11.11 μm.[15] An in vivo study in Winstar rats using optical low coherence reflectometer found a thickness of 159.08 ± 14.99 μm.[22] In our study, the average baseline CCT for all animals was 150.52 ± 31.03 μm, which is consistent with these previous studies. Overall we found corneal thickness to be the least reliable indicator of inflammation, and have concerns about the potential risk for error in CCT accuracy introduced by positioning artifact. This concern highlights one of the major challenges in longitudinal OCT image quantification in animals: the absence of image tracking for precise alignment on repeated scans. By orienting each scan on the center of the pupil, and finding the average of the entire central cornea, we attempted to minimize the potential for this error. However, further studies will be needed to refine the scan protocols to improve the quality of corneal thickness measurement.

Of note, a wide range of inflammation was identified in this study. This finding was not unexpected as other animal models of uveitis, such as EAU, also demonstrate variability in disease severity.[23–25] The model of acute anterior uveitis used in the paper is a variation of a model previously described in rabbits and rats.[16,26,27] In these published reports, uveitis is generated by an initial subcutaneous injection of a mycobacterial extract followed by intravitreal injection of the same mycobacterial extract 7 days later. Importantly, in the work described in this manuscript, uveitis was generated solely by intravitreal injection without the preceding subcutaneous injection. In our experience, the absence of the subcutaneous injection or significant variations in preparation of the mycobacterial extract contributes to increased variability in the level of inflammation. However, despite this variability, quantitative analysis of the OCT images was still able to detect a significant change in AC cell and CBI from baseline to peak inflammation and with spontaneous resolution over 14 days. This study identifies the strength of using SD-OCT for detection and monitoring inflammation in models of anterior uveitis even if they exhibit a wide range of inflammation. This study was performed using a custom OCT, but equivalent images of the AC have been obtained using the commercially available Bioptogen SR2300 system equipped with the 18-mm telecentric bore (data not shown). This study is limited by its small size and use in only a single model of anterior and intermediate uveitis. It will be important to determine how well anterior segment OCT and the quantifiable metrics of AC cell and CBI correlate with clinical and histologic scores in other common models of anterior uveitis, such as EIU or EAAU.

Acknowledgments

The authors thank Leona Ding, PhD, for her assistance with statistical analysis, and Michal Gutowski for critical reading of the manuscript.

Supported by funding from the National Institutes of Health, Bethesda, Maryland, United States (RW) R01EY024158, (KP) K08EY0123998, NIH Grant P30 EY001730 (RVG), Burroughs-Wellcome Translational Scientist Award (RVG, from the Latham Vision Science Innovation Award, the UW vision research core grant (NEI P30EY01730), the generous support of the Gensheimer family, and an unrestricted departmental grant from Research to Prevent Blindness.

Disclosure: **K.L. Pepple**, None; **W.J. Choi**, None; **L. Wilson**, None; **R.N. Van Gelder**, None; **R.K. Wang**, None

References

1. Nussenblatt RB. The natural history of uveitis. *Int Ophthalmol*. 1990;14:303–308.
2. Rothova A, Suttorp-van Schulten MS, Frits Treffers W, Kijlstra A. Causes and frequency of blindness in patients with intraocular inflammatory disease. *Br J Ophthalmol*. 1996;80:332–336.
3. Jabs DA, Nussenblatt RB, Rosenbaum JT. Standardization of uveitis nomenclature for reporting clinical data. Results of the First International Workshop. *Am J Ophthalmol*. 2005;140:509–516.
4. Margo CE, Lee A. Fixation of whole eyes: the role of fixative osmolarity in the production of tissue artifact. *Graefes Arch Clin Exp Ophthalmol*. 1995;233:366–370.
5. Chen J, Qian H, Horai R, Chan CC, Caspi RR. Use of optical coherence tomography and electroretinography to evaluate retinal pathology in a mouse model of autoimmune uveitis. *PLoS One*. 2013;8:e63904.

6. Harimoto K, Ito M, Karasawa Y, Sakurai Y, Takeuchi M. Evaluation of mouse experimental autoimmune uveoretinitis by spectral domain optical coherence tomography. *Br J Ophthalmol*. 2014;98:808–812.
7. Gadjanski I, Williams SK, Hein K, Sattler MB, Bahr M, Diem R. Correlation of optical coherence tomography with clinical and histopathological findings in experimental autoimmune uveoretinitis. *Exp Eye Res*. 2011;93:82–90.
8. Chu CJ, Herrmann P, Carvalho LS, et al. Assessment and in vivo scoring of murine experimental autoimmune uveoretinitis using optical coherence tomography. *PLoS One*. 2013;8: e63002.
9. Sharma S, Lowder CY, Vasanji A, Baynes K, Kaiser PK, Srivastava SK. Automated analysis of anterior chamber inflammation by spectral-domain optical coherence tomography. *Ophthalmology*. 2015;122:1464–1470.
10. Agarwal A, Ashokkumar D, Jacob S, Saravanan Y. High-speed optical coherence tomography for imaging anterior chamber inflammatory reaction in uveitis: clinical correlation and grading. *Am J Ophthalmol*. 2009;147:413–416.
11. Li Y, Lowder C, Zhang X, Huang D. Anterior chamber cell grading by optical coherence tomography. *Invest Ophthalmol Vis Sci*. 2013;54:258–265.
12. Choi WJ, Zhi Z, Wang RK. In vivo OCT microangiography of rodent iris. *Opt Lett*. 2014;39:2455–2458.
13. Choi WJ, Pepple KL, Zhi Z, Wang RK. Optical coherence tomography based microangiography for quantitative monitoring of structural and vascular changes in a rat model of acute uveitis in vivo: a preliminary study. *J Biomed Opt*. 2015; 20:016015.
14. Yin X, Chao JR, Wang RK. User-guided segmentation for volumetric retinal optical coherence tomography images. *J Biomed Opt*. 2014;19:086020.
15. Behar-Cohen FF, Savoldelli M, Parel JM, et al. Reduction of corneal edema in endotoxin-induced uveitis after application of L-NAME as nitric oxide synthase inhibitor in rats by iontophoresis. *Invest Ophthalmol Vis Sci*. 1998;39:897–904.
16. Pepple KL, Rotkis L, Van Grol J, et al. Primed mycobacterial uveitis (PMU): histologic and cytokine characterization of a model of uveitis in rats. *Invest Ophthalmol Vis Sci*. 2015;56: 8438–8448.
17. Pepple KL, Rotkis L, Wilson L, Sandt A, Van Gelder RN. Comparative proteomic analysis of two uveitis models in Lewis rats. *Invest Ophthalmol Vis Sci*. 2015;56:8449–8456.
18. Huang D, Swanson EA, Lin CP, et al. Optical coherence tomography. *Science*. 1991;254:1178–1181.
19. Downie LE, Stainer MJ, Chinnery HR. Monitoring of strain-dependent responsiveness to TLR activation in the mouse anterior segment using SD-OCT. *Invest Ophthalmol Vis Sci*. 2014;55:8189–8199.
20. Rosenbaum JT, McDevitt HO, Guss RB, Egbert PR. Endotoxin-induced uveitis in rats as a model for human disease. *Nature*. 1980;286:611–613.
21. Broekhuyse RM, Kuhlmann ED, Winkens HJ, Van Vugt AH. Experimental autoimmune anterior uveitis (EAAU), a new form of experimental uveitis. I. Induction by a detergent-insoluble, intrinsic protein fraction of the retinal pigment epithelium. *Exp Eye Res*. 1991;52:465–474.
22. Schulz D, Iliev ME, Frueh BE, Goldblum D. In vivo pachymetry in normal eyes of rats, mice and rabbits with the optical low coherence reflectometer. *Vision Res*. 2003;43:723–728.
23. Chen J, Qian H, Horai R, Chan CC, Falick Y, Caspi RR. Comparative analysis of induced vs. spontaneous models of autoimmune uveitis targeting the interphotoreceptor retinoid binding protein. *PLoS One*. 2013;8:e72161.
24. Mattapallil MJ, Silver PB, Cortes LM, et al. Characterization of a new epitope of IRBP that induces moderate to severe uveoretinitis in mice with H-2b haplotype. *Invest Ophthalmol Vis Sci*. 2015;56:5439–5449.
25. Klimova A, Seidler Stangova P, Svozilkova P, Forrester JV, Klaska I, Heissigerova J. The critical points in induction of experimental autoimmune uveitis. *Biomed Pap Med Fac Univ Palacky Olomouc Czech Repub*. 2016;160:140–142.
26. Mruthyunjaya P, Khalatbari D, Yang P, et al. Efficacy of low-release-rate fluocinolone acetonide intravitreal implants to treat experimental uveitis. *Arch Ophthalmol*. 2006;124:1012–1018.
27. Cousins SW. T cell activation within different intraocular compartments during experimental uveitis. *Dev Ophthalmol*. 1992;23:150–155.

Investigative Ophthalmology & Visual Science